

Hydraulic redistribution in mangroves: time-lapse electrical resistivity reveals diel patterns of subsurface salt mobilization consistent with exchange of water between trees and sediments

Christine Downs^{1,1}, Ken Krauss², and Sarah Kruse^{3,3}

¹Sandia National Laboratories

²U.S Geological Survey

³University of South Florida, Massachusetts Institute of Technology

November 30, 2022

Abstract

A 24-hour 2D time-lapse electrical resistivity imaging (ERI) survey was conducted in an altered mangrove forest on a barrier island in southeast Florida, USA, to (1) assess the method's utility in hypersaline conditions and (2) understand how trees respond to hypersaline conditions. ERI measurements serve as a proxy for pore water salinity and saturation. Here, resistivity changes suggest a lag between the tidal cycle and changes in ground resistivity. ERI data show that overall changes within 24 hours are very small, but there is more variability in resistivity in the root zone of mangroves than in open salt flat portions along a fixed transect. Two to three hours after sunset, root zone resistivity increased from initial, midday conditions. Overnight, the root zone was less resistive than midday. By sunrise, root zone resistivity was once again higher than initial conditions. Measurements from the salt flat where roots are absent remained generally constant throughout the survey. Thus, changes in resistivity over time are inferred to reflect mangrove tree physiological influences related to diel water use. A mechanistic explanation for the decreased resistivity two hours after sunset from the re-distribution of salts to the soil around the roots is the Cohesion-Tension Theory, which suggests that trees continue water uptake after sunset to balance the pressure after leaf stomates have closed. The corresponding overnight drop in ground resistivity just prior to sunrise may be explained by redistribution of freshwater from the tree to the soil that was delayed until the early morning hours. The limited period of data acquisition limits definitive data interpretations, but the study illustrates the monitoring potential of ERI in hypersaline environments such as a mangrove forest.

Hosted file

essoar.10511305.2.docx available at <https://authorea.com/users/560132/articles/608325-hydraulic-redistribution-in-mangroves-time-lapse-electrical-resistivity-reveals-diel-patterns-of-subsurface-salt-mobilization-consistent-with-exchange-of-water-between-trees-and-sediments>

Informative title: Hydraulic redistribution in mangroves: time-lapse electrical resistivity reveals diel patterns of subsurface salt mobilization consistent with exchange of water between trees and sediments

Running title: Time-lapse electrical resistivity reveals diel patterns of salt mobilization

Authors: Christine Downs¹, Sarah Kruse¹

Affiliations: ¹ University of South Florida, School of Geosciences, 4202 E Fowler Ave, Tampa, FL

Acknowledgments: Thank you to Rodney Smith, Sajad Jazayeri, Sanaz Esmaeili for assisting with fieldwork; Henok Kiflu and Peter Bumpus for assisting in fieldwork preparation. Thank you to Mark Rains for providing insight about mangrove forest dynamics; and the Smithsonian Marine Station for their generous accommodation and access to the field site. A warm thank you to Marilyn Ball for a careful, expert review of this manuscript. Any use of trade, firm, or product names is for descriptive purposes only and does not imply endorsement by the U.S. government.

Data Availability Statement: The data that support the findings of this study are available from the corresponding author upon reasonable request. If the journal offers a supplemental repository, the author will make the data available.

Abstract

A 24-hour 2D time-lapse electrical resistivity imaging (ERI) survey was conducted in an altered mangrove forest on a barrier island in southeast Florida, USA, to (1) assess the method's utility in hypersaline conditions and (2) understand how trees respond to hypersaline conditions. ERI measurements serve as a proxy for pore water salinity and saturation. Here, resistivity changes suggest a lag between the tidal cycle and changes in ground resistivity. ERI data show that overall changes within 24 hours are very small, but there is more variability in resistivity in the root zone of mangroves than in open salt flat portions along a fixed transect. Two to three hours after sunset, root zone resistivity increased from initial, midday conditions. Overnight, the root zone was less resistive than

midday. By sunrise, root zone resistivity was once again higher than initial conditions. Measurements from the salt flat where roots are absent remained generally constant throughout the survey. Thus, changes in resistivity over time are inferred to reflect mangrove tree physiological influences related to diel water use. A mechanistic explanation for the decreased resistivity two hours after sunset from the redistribution of salts to the soil around the roots is the Cohesion-Tension Theory, which suggests that trees continue water uptake after sunset to balance the pressure after leaf stomates have closed. The corresponding overnight drop in ground resistivity just prior to sunrise may be explained by redistribution of freshwater from the tree to the soil that was delayed until the early morning hours. The limited period of data acquisition limits definitive data interpretations, but the study illustrates the monitoring potential of ERI in hypersaline environments such as a mangrove forest.

Keywords: 2D, electrical resistivity, groundwater, mangrove, water uptake

Introduction

Mangrove forests are integral components of tropical and subtropical intertidal forest communities and essential to coastal stabilization and ecological processes. Due to their location between land and sea, mangrove forests play a pivotal role in climate change adaptation and mitigation. They show a great deal of ecological stability (Alongi, 2015) through their ability to elevate land surface via sediment accretion and root zone processes, often on pace with sea-level rise (Krauss et al., 2014; McIvor et al., 2013; McKee et al., 2007, 2012). They also have a strong capacity to act as CO₂ sinks (Duarte et al., 2013) while using water conservatively (Lovelock et al., 2006). Their salt tolerance lends mangroves the ability to survive harsh coastal environments (Ball, 1988; Esteban et al., 2013; Parida and Jha, 2010). Some species, like black mangroves (*Avicennia germinans*), rely on foliar salt excretion (Drennan and Pammenter, 1982; Esteban et al., 2013; Parida and Jha, 2010; Scholander et al., 1962) to prevent excess accumulation of salts not excluded when water was absorbed by roots (though black mangrove trees do filter water at the root). Excreted salt on leaves dissolves during cooler, moister periods and returns to the soil during rain events or via excised leaves. Other species, like red (*Rhizophora mangle*)

and white (*Laguncularia racemosa*) mangroves, exclude more salt at the roots. During water uptake, water must move down from the soil surface to the roots. By convection, salt also moves down and is then excluded by roots, thus contributing to a local soil salinity maxima directly in the rhizosphere—the region of soil directly influenced by plant root activity (Passioura et al., 1992). While the salt balance in a given tree is presumably maintained, the subsurface can experience gains in salt concentration over time unless upward diffusion of salt balances the downward convection.

Trees may hydrate via foliar absorption of atmospheric water, which can bring more water into the tree than root water uptake alone. This top-down rehydration can ultimately lead to fresh water discharge into the soil. Hao et al. (2009) suggested hydraulic redistribution to explain lower salinities in the root zones of scrub *Rhizophora mangle* that are growing in an area perennially flooded with seawater. Hydraulic redistribution has been demonstrated in many plants of upland ecosystems. Coopman et al. (2021) showed that the capacity of a salt-secreting mangrove (*Avicennia marina*) to access water from an unsaturated atmosphere demonstrates top-down hydration at scales and frequencies of major consequence to tree function under hypersaline conditions. This prompts the questions about the extent and timing of effects of top-down rehydration on soil pore water salinity.

Tidal forcing is typically the dominant mechanism of pore water and salt movement in the saturated and intertidal zones of coastal wetlands and can remove locally excess salt caused by mangrove tree activity (Hughes et al., 1998; Sam and Ridd, 1998; Wolanski et al., 1993). However, the construction of impoundments alters the salinity balance maintained under natural conditions, and, globally, mangroves suffer from tidal restrictions that influence their ecological function and sometimes lead to rapid mortality once multiple stress thresholds are exceeded (Lewis et al., 2016). Impoundments can be earthen dikes that surround sections of forest and hydrologically isolate them from tidal surface water and each other, which can lead to concentrated salinities to levels deleterious even to mangroves. In these cases, evapotranspiration (ET) can become the most influential factor in determining pore water salinities and stand stress, particularly during hot, dry periods

(Stringer et al., 2010).

While the concept of root zone salinity concentration with prolonged daily water uptake and ultrafiltration is theoretically tenable, it is important to document how changes in salinity distribution relate to specific tidal and sunrise/sunset cycles in actual mangrove forests. Transpiration significantly decreases at night when photosynthetically active radiation is eliminated, and air temperatures drop. At this time, the water potential in the roots will rise to slow down or cease the intake of soil water. At the start of the day, transpiration resumes, and the root's water potential drops to facilitate root water uptake. Transpiration in mangroves reaches a maximum rate around midday, but maximum cumulative amounts of water transited each day would be realized slightly after sunset as water uptake continues even after stomates (leaf 'pores') are likely closed (Krauss et al., 2007).

This study focuses on an impounded portion of a mangrove forest on a barrier island in east-central Florida, where the forest is isolated from tidal inundation (**Error! Reference source not found.**). The impoundment was initially constructed for mosquito abatement. It is comprised of an earthen dike that run along the water's edge and inland to break up the forest into sections. A pump/culvert system is installed within the dike connecting the lagoon to a ditch on the interior side of the dike. In the past, the culvert was a free opening for water to flow through the dike when water levels were high enough. Current water management practices pump brackish water into the impoundment to keep it inundated from April to October to simulate more natural conditions. The impoundment area is then allowed to dry up entirely from November to March.

The trees are predominantly black mangroves and most (90%) porewater salt is excluded during water uptake by the roots. The salt that is transported to the shoot either becomes stored for osmotic adjustment or developing tissues. Excess salt is expelled from the leaves via salt excretion glands (Ball et al., 1988). Impoundment practices can decrease mangrove growth rates and diversity (Berrenstein et al., 2013; Brockmeyer Jr et al., 1996; Crase et al., 2013; Harris et al., 2010; Middleton et al., 2008; Rey et al., 2009, 1990; Rey and Rutledge, 2009), which may imply nutrient limitations, prolonged flooding, and soil

hypersalinity within the rhizosphere. In fact, it is typically expected that zones with the most active roots have the highest salinity concentrations (Passioura et al., 1991) with levels increasing until the rate of convection transport to the roots equal the rate of diffusive transport to the surface sediment. Stringer and others (2010) hypothesized that, in the impoundment of interest, dense, saline pore water in these active zones sinks to create a hypersaline layer 1-4 m below the mangrove and ecophysiological processes within mangrove vegetation such as hydraulic lift (e.g., Dawson, 1993) interact with this layer to alter salinity concentration within the rhizosphere over a daily transpirational cycle. However, in the absence of mangrove activity as ions diffuse along a concentration gradient toward the soil surface such a hypersaline layer would presumably collapse.

We take a geophysical approach to detect spatial and temporal variation in salinity profiles that would reflect diel signatures of water uptake by the trees and hydraulic redistribution of atmospherically-sourced fresh water from the trees into the soil. Time-lapse electrical resistivity imaging (ERI) has proven useful in imaging changes in soil moisture and root uptake (e.g., Beff et al., 2013; Brillante et al., 2016; Consoli et al., 2017; Daily et al., 1992; Garré et al., 2011; Lewis et al., 2016; Mares et al., 2016; Mary et al., 2020; Musgrave and Binley, 2011), the mobility of saline tracers (e.g., Binley et al., 1996; Cassiani et al., 2006; Kemna et al., 2002; Robinson et al., 2020; Singha and Gorelick, 2005; Slater et al., 1997; Slater and Sandberg, 2000) or contaminants (e.g., Hayley et al., 2009; Mansoor and Slater, 2007), and changes in both soil moisture and salinity in saline environments (Attwa et al., 2011; Boaga et al., 2014; Brindt et al., 2019; deFranco et al., 2009; Kiflai et al., 2020; Leroux and Dahlin, 2006; Slater and Sandberg, 2000; Sutter and Ingham, 2016; Urish and Frohlich, 1990; Vacher et al., 2008). This paper reports on the observations made with a time-lapse ERI survey coupled with real-time groundwater data and tidal records. Our objectives were to assess (1) the effectiveness of ERI under hypersaline conditions and (2) the spatiotemporal changes in saline pore water structures as a function of diel and tidal cycles in the absence of surface interaction between the impounded mangrove forest and lagoon. Interpretations were made with consideration given to what is already known about mangrove tree physiological processes in unaltered mangrove forests.

Field Site

Imp-24 is a mosquito-control impoundment on the west side on North Hutchinson Island, Florida, USA (Figure 1 top). North Hutchinson Island is a siliciclastic barrier island approximately 35 km long and 0.7 km wide. The Indian River Lagoon, a tidal estuarine system, borders the west shore of the island; the Atlantic Ocean borders the east side. The lagoon connects to the Atlantic Ocean about 9 km south of Imp-24, and a lagged and dampened tidal signature is observed in the ditch between the impoundment and the lagoon compared to the semidiurnal tidal regime observed at the lagoon's opening.

For the Indian River Lagoon, average precipitation rates are 1,180 mm/yr (Sumner and Belaine, 2005). Open water evaporation rate is 1,502–1,614 mm/yr, with the lowest rate occurring in the winter months (District, 2006; Sumner and Belaine, 2005). Vegetated areas experience an estimated 2.6 to 3.5 mm/day (967–1,278 mm/yr) of evapotranspiration based on similar basin mangrove types in the region (Lugo et al., 1975; Twilley and Chen, 1998). Mangrove evapotranspiration (ET) rates strongly influence pore water salinities (Esteban et al., 2013), and changes in water management practices in the mangrove forest have also produced changes in the pore water salinity structure. The vegetation and surface water are separated from the neighboring lagoon by an earthen dike. Maximum water levels are maintained during the summer season (~0.6 m, April-October) and allowed to dry during the winter (November-March) (Connelly and Carlson, 2009; Middleton et al., 2008; Rey and Rutledge, 2009). In the dry season, pore water salinities are more heavily affected by ET rates (Stringer et al., 2010), which lowers the water table and creates a gradient that drives lagoon water to the mangrove via groundwater flow (Figure 1 bottom).

We established a transect through a high-salinity and small-stature mangrove forest. The very shallow subsurface along the resistivity transect can be partitioned into three vegetative zones (Figure 2 top). From the western end to seven meters along the transect, the surface is dominated by dense, height-restricted scrub mangroves. The central portion is a salt flat with standing roots only along the edges. At the center of the salt flat (about 30 m along the transect), there is a small scrub mangrove patch very near the transect. In a sense, much of the salt flat serves as a control area where the influence from root activity is

presumably absent. From 40 m along the transect to the eastern end, the vegetation is characterized by sparse, scrub trees. Digging in the vicinity of trees shows the root zones of dense tree groupings extend as far as 1.5 meters in depth. Shallow sediments are fine-grained sand composed of quartz and calcareous grains (Stringer et al., 2010).

Methods

With an AGI Supersting R8 resistivity meter, we performed repeated electrical surveys over 24 hours (March 27–28, 2015) at the end of the "dry" season. Fifty-six electrodes remained stationary throughout the survey. It was important to have high lateral sensitivity in the root zone (0–2 m depth) and moderate vertical sensitivity in the top two meters. Thus, a combined dipole-dipole inverse Schlumberger array configuration with a 1-meter dipole spacing was chosen. Each survey took approximately 45 minutes. To capture both diel and tidal effects on salinity structures in the sub-surface, a 2-D transect array was collected approximately every hour for 24 hours starting at about noon on day 1. Gaps exist in our acquisition schedule due to battery issues. Nevertheless, there is at least one data set representing four diel-tidal combinations—daytime, low tide; daytime, high tide; nighttime, low tide; nighttime, high tide. The first survey acquired 1219 quadripoles; subsequent surveys collected 1045 to 1146 quadripoles for a total of 13,890.

There was standing water at certain times on the western half of the array, so electrodes were cased in PVC pipes pushed approximately 3 cm into the ground to avoid losing current to surface water. Contact resistance tests confirmed the ground was wet enough to deem watering the electrodes with saltwater unnecessary. Relief along the transect, as observed in a LiDAR-derived digital elevation model, is extremely subtle (0.07 m). For this reason, topography was not included in the inversion.

As in any ER study, it is necessary to assess measurement error before data inversion and interpretation. Following the repeat measurement error assessment of Brindt et al. (2019) and Mares et al. (2016), for example, measurements with an acquisition error above 2% were removed (Figure 2 bottom). Of the 13,890 quadripoles collected, 13,573 were used in the inversion.

The resistivity data were inverted with ResIPy, an open-source geoelectric inversion and modeling software (Blanchy et al., 2020). The models were parameterized on a triangular mesh with the finest node spacing closest to the surface (~ 0.25 m) and progressively coarser spacing (~ 1 m) with depth. The first time step was inverted using a uniform reference model of $100 \Omega\text{m}$. Time-lapse inversion is preferred because outliers or noise inherent in each dataset has less influence in the solution versus individual solutions (Binley et al., 1996; Loke, 2014). Time steps were regularized relative to the first dataset to prioritize smoothing changes from one dataset to the next. When the inversion was complete, data points that had a misfit beyond $\pm 3\%$ were filtered out, and the data were inverted again.

Direct groundwater data were also collected using Decagon conductivity, temperature, and water depth sensors (CTD) deployed down PVC wells. The PVC wells, installed four months earlier, were screened at 0.6 m and 1.2 m and resided at the western edge of the transect. Sensors were calibrated at the start of the first day of sampling with room temperature with tap water. The sensors recorded measurements at 15-minute intervals throughout the ERI survey. Due to equipment failure, only water conductivity and one set of temperature readings are presented.

Results and Discussion

The depth of investigation (DOI) was assessed using the method described by Oldenburg and Li (1999), where the first time step is inverted using two different reference resistivities (0.06 and $5.69 \Omega\text{m}$). These reference values were based on the average observed apparent resistivity values. Considering a cautious DOI index cutoff of 0.1 , our maximum depth of investigation is about 5 m with the exception of the first 2 m along the array. The true resolution matrix (Figure 3) (Binley and Kemna, 2005, Eq. 5.18) shows inverted resistivity is best resolved in the first 1 - 2 meters, which is suitable for imaging changes in the root zone of mangrove trees. Accordingly, only the top 2 m of resistivity profiles are presented and discussed.

The inversion results yield zones with near-electrode values that locally alternate

between relatively high and low resistivity, particularly at electrodes placed in between tree roots. This is likely due to noisy data as a result of poor contact between electrodes and sediment. Since noise appears to be an issue in vegetated zones and not the open salt plan, the roots themselves may contribute to poor electrode contact. Small burrowing animals (e.g., fiddler crabs; Ocypodidae) are common in the forest and the distribution of their burrows, which would contribute to poor contact, may be concentrated in the root zone. It is also worth noting that burrowing animal activity also alters local mud chemistry due to enhanced diffusive exchange of dissolved material between the surface and porewater through the sediment surface (Smith et al., 1991).

Since inversion results suffer from near-electrode artifacts, and reciprocal readings were not collected due to time constraints, we present first-order trends and patterns between time-lapse inversion results and environmental changes as measured in ancillary data. Terrain resistivity is controlled by temperature, ground saturation, matrix properties, and groundwater salinity. Results are presented in terms of change from the first time step, thus removing the signature of presumably static matrix properties. The remaining parameters are discussed in turn.

The ground temperature at 0.6 m depth was 22° C at the start of the survey and decreased to 21° C by the end of the survey (Figure 4 bottom). This temperature decrease corresponds to a 2% apparent resistivity increase, which is small but so are resistivity changes between time steps. We use the linear temperature-dependent model from Hayley et al. (2007) and the fractional change coefficient ($m=0.0187$) by Hayashi (2004) to calculate the effect of groundwater temperature at 0.6 m on electrical resistivity measurements. Ground temperature was measured at 15-minute intervals. For a given ERI time step, we averaged ground temperature measurements collected over the duration of a given ERI acquisition time. The temperature-dependent model was applied to each ERI time step using these average values and 22°C as the standard value.

Terrain resistivity is expected to be inversely proportional to the degree of groundwater saturation (e.g., Archie, 1942). There were approximately 4 cm of standing water at the western end of the transect at the start of the study. Surface water levels along

this western end gradually dropped until there was no standing water, and did not return through the course of the 24-hour recording period, as would have been expected had the local surface water levels tracked the tidal cycle recorded at the pump station in the trench between the earthen dike and mangrove forest (Locer, 2016) (Figure 4 top). The portion of the forest where the survey took place is thus far enough inland to have not been completely inundated during high tide, and the saturation pattern is not readily correlated with tides. It had rained 18 hours before the study, and standing water levels might also reflect local lateral surface water perching and flow. The ground appeared highly saturated throughout to the end of the study, in the sense that augered holes showed full saturation at depths less than 10 cm.

Pore water resistivity at 0.6 m depth and 1.2 m depth are compared with the mean apparent resistivity from the top 2 meters and easternmost 5 meters along the ERI transect of each time step (Figure 4, middle and bottom, respectively). The ranges of measurement values from 0.6 m and 1.2 m depths are 0.15-0.18 Ωm and 0.12-0.13 Ωm , respectively. This is a narrower range than that of apparent resistivities (0.01 – 9.23 Ωm) from the west end of the profile. A formation factor is the ratio of the resistivity of water-filled rock or sediment to that of the water and is often used to describe porosity or at least expected porosity for a given geomaterial (Archie, 1942). An average formation factor is estimated here by taking the ratio between water resistivity at 0.6 m depth and the inverted resistivity value for the model cells closest to the location of the 0.6 m well at the east end of the array. Both groundwater conductivity and inverted terrain resistivity were averaged over the diel period, to yield a formation factor of 4.8. This differs from the previous estimate of 3.6 by Stringer et al. (2010), which was based on electromagnetic measurements of terrain conductivity with larger sampling volumes. It has been shown that the formation factor varies spatially and temporally (Singha and Gorelick, 2005), so it is reasonable—and expected—to resolve a range of values at a local scale. The 4.8 value is within the range of published formation factors for sandy soils, such as found at the study site.

Temporal variations in pore water conductivity recorded over the diel period at the wells at 0.6 m and 1.2 m are quite small and not synchronous (Figure 5, middle and

bottom). Measurements (converted from conductivity to resistivity for comparative purposes) at 0.6 m correspond to salinities between 38 and 41 psu (Fofonoff and Millard, 1983). Measurements at 1.2 m correspond to above-seawater salinities and are beyond the range of valid values for converting to salinity. The sum of apparent resistivity from each time step is compared to air temperature as well (Figure 5), which helps make inferences about the relationship between ground salinity and saturation and factors that influence ET. Resistivity values for the entire time-lapse survey range from 0.13 to 2600 Ωm . The median resistivity is 2.8 Ωm ; the standard deviation is 1.6 Ωm . Figure 6 shows the change a resistivity between a given time step and the first time step. The values between time steps are quite noisy, as they are relatively small compared to the overall signature. In this study, we focus on first-order trends as they relate to diel and tidal stages within the vegetation zone.

Root zone

Overall, the root zones are more resistive than the neighboring salt flat as expected as roots ameliorate salinity conditions (Figure 6, left column). This applies to the tree groupings on the east and west ends of the resistivity profile and the single shrub in the middle of the profile (Figure 2 top). The patch of standing roots extending out from the western tree grouping away from the forest canopy to about 15 m along the transect is also consistently more resistive than the rest of the salt flat.

We present the difference in inverted resistivity between selected time steps and the initial model at 13:00 during a rising tide (Figure 6, right column). The median difference from the initial model (for all time steps) is 0.22 Ωm , the interquartile range is 0.47 Ωm , and the standard deviation is 1.69 Ωm . Outliers concentrated near selected electrodes are likely due to loss of contact between the electrode and the soil. These values are not shown in Figure 6.

The western tree grouping, including the standing roots extending 15 m into the salt flat, experienced an increase in resistivity (0.5 to 1.3 Ωm increase) from the afternoon until after sunset (22:00) when the tide was falling. This portion of the profile then becomes

progressively less resistive until 03:30 (rising tide) when the area is 0.5 to 2 Ωm less resistive than the initial state. From 05:00 to 07:00, conditions are essentially the same as the initial state. After sunrise (08:00 to 11:00), the western tree grouping and standing roots are once again more resistive than the initial conditions though not to the same extent as the previous afternoon and evening.

The single shrub in the middle of the salt flat presents a similar trend. Conditions are more resistive than the initial state through the afternoon and early evening. Resistivity decreases until the early morning hours when conditions are similar to or less resistive than the initial state. The area is once again more resistive after sunrise. The eastern tree grouping consistently yields very large changes from the initial model. Although outliers are present, the overall trend suggests the area is more resistive than initial conditions during the day and less resistive overnight.

Interpretations

The temporal changes in the resistivity profiles are on the same scale as those in the measured groundwater conductivities over the diel period (Figure 4); however, they do not necessarily follow the same trend. Such small changes in ground conductivities, as measured in the ER data, fall in the envelope of instrument error (± 0.01 mS/cm or $\pm 1\text{e}3$ Ωm .) The overall values do yield a plausible formation factor, and the higher pore water resistivities recorded at 0.6-meter depth over those at 1.2-meters depth agree with the distribution recorded in the resistivity surveys. The terrain resistivity data are robust in that they agree with the observed geological structure and show general trends that can be interpreted.

In a coastal environment, one can expect shallow terrain resistivities to be their lowest at high tide when tidal forcing increases the extent of brackish water ingress. Although the impoundment does not experience tidal inundation, we considered any signature of tidal forcing. In this study, the lowest resistivities are observed overnight after high tide as the tide is falling (Figure 4; Figure 6, right column). This would indicate that the tidal cycle does influence ground resistivity and that there is a time lag between high

344 tide and minimum ground resistivity. On the other hand, the same pattern is not observed
345 before sunset when the tide is also falling. Furthermore, this pattern is not captured by
346 direct groundwater measurements. Thus, our observations do not appear to support tidal
347 cycles as the sole controller of the observed resistivity cycle. We consider instead that our
348 ER data are, at least partially, controlled by pore water conductivity and saturation changes,
349 which are, to some extent, controlled by tree activity and varies with the time of day.

350 Low water pressure potential in roots creates an upward hydraulic gradient during
351 daylight hours. Black mangrove trees partially filter salts at the root during water uptake
352 and excrete excess salt from the leaves during transpiration. Transpiration rates of south
353 Florida mangrove trees slow down with stomatal closure at sundown, but upward stem
354 water movement (sap flow) continues one to two hours in many tree species after sunset
355 as continued water absorption is required for rehydration of tissues in an effort to balance
356 the pressure well after stomates are closed (Meinzer et al., 2004). Black mangroves
357 growing in scrub environments of Louisiana, USA continue to take water up for at least an
358 hour or more after sunset (Krauss et al., 2014). The water pressure gradient in a tree is
359 inversely proportional to its water content. Accordingly, the sustained upward sap flow can
360 continue until the pressure gradient between soil pore water and the tree collapses.
361 Recharge of the soil possible if the tree achieves a higher water potential than that of pore
362 water around the roots. A possible scenario for this could be the uptake of water from roots
363 at shallow soil depths where pore water salinity is lower than that of soil pore water
364 surrounding roots at greater soil depths. This may lead to a downward transfer, via reverse
365 sap flow, of low salinity water extracted from shallow soil depths and transported through
366 the tree into greater soil depths. Whether reverse sap flow occurs or not, transpiration
367 resumes at sunrise prompting the upward hydraulic gradient once again.

368 If we consider this cycle in terms of the resistivity results, some patterns emerge.
369 Relative to the first time step at 15:00, the root zone became more resistive in the late
370 afternoon before sunset (Figure 6, right column). These conditions continued— though a
371 slight decrease in resistivity is present after sunset (19:30)— until approximately midnight.
372 Recall that black mangrove trees exclude 90% of pore water salts during water uptake. We

attribute the increased resistivity to continual water uptake of filtered water stranding salts in the rhizosphere, suggesting the ER response is from a combination of declining water content and increased soil salinity. The trend continues throughout the first half of the night as sap flow is known to also continue. Boaga et al. (2014), for example, also show that water uptake in the root zone can produce pockets of more resistive ground even when the surface is flooded.

From about midnight to sunrise, the ground is overall less resistive than initial conditions. The largest decreases occurring in vegetated areas. The salt flat is only slightly less resistive than initial conditions (about $-0.25 \Omega\text{m}$) and the change is very uniform. In a sense, the salt flat where roots are completely absent serve as a control area. We attribute the larger decrease in resistivity to water uptake ceasing and even freshwater recharge to the area around trees via reverse sap flow (e.g. Coopman et al., 2021). Again, this suggests that varying water content is driving the ER signal.

Ground conditions are once again more resistive than initial conditions by sunrise (07:30). The pattern in increased resistivity is similar to that pre-sunset with the most significant changes occurring in vegetated and standing root areas. These conditions continue through to the end of the survey (11:00). We attribute this to transpiration resuming, prompting an upward hydraulic gradient and water uptake.

The suggestion of water returning to the soil via tree roots is the process known as hydraulic redistribution that has been observed in dry environments (Caldwell et al., 1998; Caldwell and Richards, 1989; Ludwig et al., 2003; Richards and Caldwell, 1987), temperate forests (Meinzer et al., 2004), savannas (Meinzer et al., 2004; Scholz et al., 2002) and mangrove forests (Hao et al., 2009). Hao and others (2009) found that reverse flow in dwarf red mangroves in south Florida may help to relieve the adverse effects of hypersaline conditions in a given tree. Our results support this process. While the hypersaline conditions in the impounded mangrove forest discuss here are detrimental to mangrove tree growth, hydraulic redistribution may be an important factor in addition to salt exclusion and salt excretion for its survival (Figure 7).

The mangrove trees may then reverse their pressure gradient overnight rather than simply reduce water uptake completely and redistribute freshwater to the root zone slowly thereafter, perhaps in combination with high tide. Such a phenomenon would indicate mangrove trees benefit from hydraulic redistribution overnight to offset maximum transpiration-imposed root zone salinity increases by the end of the day and into the early part of the evening. This would require an alternative source of water, specifically uptake of atmospheric water.

Our study tests the ability of electrical resistivity to detect small changes in ground resistivity in a hypersaline environment. The observations presented here are temporally finite. It is not possible to make inferences about seasonal or annual patterns or even average daily processes. Nevertheless, the data indicate a tidal influence compounded with mangrove tree physiological processes, understanding of which ultimately assists in assessing the long-term effects of diking on mangrove forests.

Conclusions

We evaluate the use of repeat electrical resistivity surveys to image changing ground conditions in a hypersaline mangrove environment. Time-lapse electrical resistivity surveys capture dynamic processes within the root zone of a mangrove forest over a diel cycle and appear to reflect tree physiological processes and tidal forcing. We infer that the mangrove trees in an impounded forest on a barrier island may pull saline water up from the root zone during the day and for a time after sunset. The data suggest that this process reverses overnight when fresher water is returned to the soil via hydraulic redistribution. The period over which data acquisition took place limits data interpretations and the data appears to suffer from noise due to questionable contact between electrodes and sediment. Nevertheless, this study presents the utility of ER in monitoring plant-soil interactions in hypersaline environments, such as a mangrove forest.

References

Alongi, D.M., 2015. The impact of climate change on mangrove forests. *Curr. Clim. Chang. Reports* 1, 30–39.

429 Archie, G.E., 1942. The electrical resistivity log as an aid in determining some reservoir
430 characteristics. *Trans. AIME* 146, 54–62.

431 Attwa, M., Günther, T., Grinat, M., Binot, F., 2011. Evaluation of DC, FDEM and IP
432 resistivity methods for imaging perched saltwater and a shallow channel within coastal
433 tidal flat sediments. *J. Appl. Geophys.* 75, 656–670.
434 <https://doi.org/10.1016/j.jappgeo.2011.09.002>

435 Ball, M.C., 1988. Ecophysiology of mangroves. *Trees* 2, 129–142.

436 Beff, L., Günther, T., Vandoorne, B., Couvreur, V., Javaux, M., 2013. Three-dimensional
437 monitoring of soil water content in a maize field using electrical resistivity
438 tomography. *Hydrol. Earth Syst. Sci.* 17. <https://doi.org/10.5194/hess-17-595-2013>

439 Berrenstein, H.J., Mans, D.R.A., Bhansing, M., Wakiran, W.S., Atmopawiro, S.L.,
440 Chotkan, N.R., Karsoredjo, R.S., Sabiran, S.A., 2013. Effects of diking on the
441 biological performance of the black mangrove (*Avicennia germinans* L.) in an Atlantic
442 mangrove forest. *Wetl. Ecol. Manag.* 21, 165–172.

443 Binley, A., Henry-Poulter, S., Shaw, B., 1996. Examination of solute transport in an
444 undisturbed soil column using electrical resistance tomography. *Water Resour. Res.* 32,
445 763–769.

446 Binley, A., Kemna, A., 2005. DC Resistivity and Induced Polarization Methods, in:
447 *Hydrogeophysics*. https://doi.org/10.1007/1-4020-3102-5_5

448 Blanchy, G., Saneiyani, S., Boyd, J., McLachlan, P., Binley, A., 2020. ResIPy, an intuitive
449 open source software for complex geoelectrical inversion/modeling. *Comput. Geosci.*
450 <https://doi.org/10.1016/j.cageo.2020.104423>

451 Boaga, J., D’Alpaos, A., Cassiani, G., Marani, M., Putti, M., 2014. Plant-soil interactions in
452 salt marsh environments: Experimental evidence from electrical resistivity
453 tomography in the Venice Lagoon. *Geophys. Res. Lett.* 41.
454 <https://doi.org/10.1002/2014GL060983>

455 Brillante, L., Bois, B., Mathieu, O., Lévêque, J., 2016. Electrical imaging of soil water

456 availability to grapevine: a benchmark experiment of several machine-learning
 457 techniques. *Precis. Agric.* 17. <https://doi.org/10.1007/s11119-016-9441-1>
 458 Brindt, N., Rahav, M., Wallach, R., 2019. ERT and salinity – A method to determine
 459 whether ERT-detected preferential pathways in brackish water-irrigated soils are
 460 water-induced or an artifact of salinity. *J. Hydrol.* 574.
 461 <https://doi.org/10.1016/j.jhydrol.2019.04.029>
 462 Brockmeyer Jr, R.E., Rey, J.R., Virnstein, R.W., Gilmore, R.G., Earnest, L., 1996.
 463 Rehabilitation of impounded estuarine wetlands by hydrologic reconnection to the
 464 Indian River Lagoon, Florida (USA). *Wetl. Ecol. Manag.* 4, 93–109.
 465 Caldwell, M.M., Dawson, T.E., Richards, J.H., 1998. Hydraulic lift: consequences of water
 466 efflux from the roots of plants. *Oecologia* 113, 151–161.
 467 Caldwell, M.M., Richards, J.H., 1989. Hydraulic lift: water efflux from upper roots
 468 improves effectiveness of water uptake by deep roots. *Oecologia* 79, 1–5.
 469 Cassiani, G., Bruno, V., Villa, A., Fusi, N., Binley, A., 2006. A saline trace test monitored
 470 via time-lapse surface electrical resistivity tomography. *J. Appl. Geophys.* 59, 244–
 471 259.
 472 Connelly, C.R., Carlson, D.B. (Eds.), 2009. Florida Mosquito Control: The state of the
 473 mission as defined by mosquito controllers, regulators, and environmental managers.,
 474 Florida Co. ed. University of Florida, Institute of Food and Agriculture Sciences,
 475 Florida Medical Entomology Laboratory, Vero Beach, FL.
 476 Consoli, S., Stagno, F., Vanella, D., Boaga, J., Cassiani, G., Roccuzzo, G., 2017. Partial
 477 root-zone drying irrigation in orange orchards: Effects on water use and crop
 478 production characteristics. *Eur. J. Agron.* <https://doi.org/10.1016/j.eja.2016.11.001>
 479 Coopman, R.E., Nguyen, H.T., Mencuccini, M., Oliveira, R.S., Sack, L., Lovelock, C.E.
 480 and Ball, M.C., 2021. Harvesting water from unsaturated atmospheres: deliquescence
 481 of salt secreted onto leaf surfaces drives reverse sap flow in a dominant arid climate
 482 mangrove, *Avicennia marina*. *New Phytologist*, 231(4), pp.1401-1414.

483 Crase, B., Liedloff, A., Vesk, P.A., Burgman, M.A., Wintle, B.A., 2013. Hydroperiod is the
484 main driver of the spatial pattern of dominance in mangrove communities. *Glob. Ecol.*
485 *Biogeogr.* 22, 806–817.

486 Daily, W., Ramirez, A., LaBrecque, D., Nitao, J., 1992. Electrical resistivity tomography of
487 vadose water movement. *Water Resour. Res.* 28, 1429–1442.
488 <https://doi.org/10.1029/91WR03087>

489 Dawson, T.E., 1993. Hydraulic lift and water use by plants: implications for water balance,
490 performance and plant-plant interactions. *Oecologia* 95.
491 <https://doi.org/10.1007/BF00317442>

492 deFranco, R., Biella, G., Tosi, L., Teatini, P., Lozej, A., Chiozzotto, B., Giada, M.,
493 Rizzetto, F., Claude, C., A., M., and Bassan, V., Gasparetto-Stori, G., 2009.
494 Monitoring the saltwater intrusion by time lapse electrical resistivity tomography: The
495 Chioggia test site (Venice Lagoon, Italy). *J. Appl. Geophys.* 69, 117–130.
496 <https://doi.org/10.1016/j.jappgeo.2011.08.004>

497 District, S.J.R.W.M., 2006. Evaluation of potential impact of demineralization
498 concentration discharge to the Indian River Lagoon (study).

499 Drennan, P., Pammenter, N.W., 1982. Physiology of salt excretion in the mangrove
500 *Avicennia marina* (Forsk.) Vierh. *New Phytol.* 91, 597–606.

501 Duarte, C.M., Losada, I.J., Hendriks, I.E., Mazarrasa, I., Marbà, N., 2013. The role of
502 coastal plant communities for climate change mitigation and adaptation. *Nat. Clim.*
503 *Chang.* 3. <https://doi.org/10.1038/NCLIMATE1970>

504 Esteban, R., Fernández-Marín, B., Hernandez, A., Jiménez, E.T., León, A., García-
505 Mauriño, S., Silva, C.D., Dolmus, J.R., Dolmus, C.M., Molina, M.J., Others, 2013.
506 Salt crystal deposition as a reversible mechanism to enhance photoprotection in black
507 mangrove. *Trees* 27, 229–237.

508 Fofonoff, N.P., Millard, R.C., 1983. Algorithms for computation of fundamental properties
509 of seawater. *UNESCO Tech. Pap. Mar. Sci.* 44. <https://doi.org/10.1111/j.1365->

2486.2005.001000.x

- Garré, S., Javaux, M., Vanderborght, J., Pagès, L., Vereecken, H., 2011. Three-dimensional electrical resistivity tomography to monitor root zone water dynamics. *Vadose Zo. J.* <https://doi.org/10.2136/vzj2010.0079>
- Hao, G.-Y., Jones, T.J., Luton, C., Zhang, Y.-J., Manzane, E., Scholz, F.G., Bucci, S.J., Cao, K.-F., Goldstein, G., 2009. Hydraulic redistribution in dwarf *Rhizophora* mangle trees driven by interstitial soil water salinity gradients: impacts on hydraulic architecture and gas exchange. *Tree Physiol.* 29, 697–705.
- Harris, R.J., Milbrandt, E.C., Everham III, E.M., Bovard, B.D., 2010. The effects of reduced tidal flushing on mangrove structure and function across a disturbance gradient. *Estuaries and coasts* 33, 1176–1185.
- Hayashi, M., 2004. Temperature-electrical conductivity relation of water for environmental monitoring and geophysical data inversion. *Environ. Monit. Assess.* 96, 119–128. <https://doi.org/10.1023/B:EMAS.0000031719.83065.68>
- Hayley, K., Bentley, L.R., Gharibi, M., 2009. Time-lapse electrical resistivity monitoring of salt-affected soil and groundwater. *Water Resour. Res.* 45. <https://doi.org/10.1029/2008WR007616>
- Hayley, K., Bentley, L.R., Gharibi, M., Nightingale, M., 2007. Low temperature dependence of electrical resistivity: Implications for near surface geophysical monitoring. *Geophys. Res. Lett.* 34.
- Hughes, C.E., Binning, P., Willgoose, G.R., 1998. Characterisation of the hydrology of an estuarine wetland. *J. Hydrol.* 211, 34–49.
- Kemna, A., Vanderborght, J., Kulesa, B., Vereecken, H., 2002. Imaging and characterisation of subsurface solute transport using electrical resistivity tomography ERT and equivalent transport models. *J. Hydrol.* 267, 125–146.
- Kiflai, M.E., Whitman, D., Ogurcak, D.E., Ross, M., 2020. The Effect of Hurricane Irma Storm Surge on the Freshwater Lens in Big Pine Key, Florida using Electrical

537 Resistivity Tomography. *Estuaries and Coasts* 43. <https://doi.org/10.1007/s12237-019->
538 00666-3

539 Krauss, K.W., McKee, K.L., Lovelock, C.E., Cahoon, D.R., Saintilan, N., Reef, R., Chen,
540 L., 2014. How mangrove forests adjust to rising sea level. *New Phytol.* 202, 19–34.

541 Krauss, K.W., Young, P.J., Chambers, J.L., Doyle, T.W., Twilley, R.R., 2007. Sap flow
542 characteristics of neotropical mangroves in flooded and drained soils. *Tree Physiol.*
543 27, 775–783.

544 Leroux, V., Dahlin, T., 2006. Time-lapse resistivity investigations for imaging saltwater
545 transport in glaciofluvial deposits. *Environ. Geol.* 49, 347–358.
546 <https://doi.org/10.1007/s00254-005-0070-7>

547 Lewis, R.R., Milbrandt, E.C., Brown, B., Krauss, K.W., Rovai, A.S., Beever, J.W., Flynn,
548 L.L., 2016. Stress in mangrove forests: Early detection and preemptive rehabilitation
549 are essential for future successful worldwide mangrove forest management. *Mar.*
550 *Pollut. Bull.* 109. <https://doi.org/10.1016/j.marpolbul.2016.03.006>

551 Locer, E., 2016. Locer Environmental [WWW Document]. URL
552 <http://data.locherenv.com/vdv/index.php>

553 Loke, M.H., 2014. Time-lapse resistivity imaging inversion, in: 5th EEGS-ES Meeting.
554 <https://doi.org/10.3997/2214-4609.201406397>

555 Lovelock, C.E., Ball, M.C., Feller, I.C., Engelbrecht, B.M.J., Ewe, M.L., Ling Ewe, M.,
556 2006. Variation in hydraulic conductivity of mangroves: influence of species, salinity,
557 and nitrogen and phosphorus availability. *Physiol. Plant.* 127, 457–464.

558 Ludwig, F., Dawson, T.E., de Kroon, H., Berendse, F., Prins, H.H.T., 2003. Hydraulic lift
559 in *Acacia tortilis* trees on an East Africansavanna. *Oecologia* 134, 293–300.

560 Lugo, A.E., Evink, G., Brinson, M.M., Broce, A., Snedaker, S.C., 1975. Diurnal rates of
561 photosynthesis, respiration, and transpiration in mangrove forests of south Florida, in:
562 Golley, F.B., Medina, E. (Eds.), *Tropical Ecological Systems*, Vol. 11. Springer, pp.

335–350. https://doi.org/https://doi.org/10.1007/978-3-642-88533-4_22

Mansoor, N., Slater, L., 2007. Aquatic electrical resistivity imaging of shallow-water wetlands. *Geophysics* 72, F211–F221.

Mares, R., Barnard, H.R., Mao, D., Revil, A., Singha, K., 2016. Examining diel patterns of soil and xylem moisture using electrical resistivity imaging. *J. Hydrol.* 536. <https://doi.org/10.1016/j.jhydrol.2016.03.003>

Mary, B., Peruzzo, L., Boaga, J., Cenni, N., Schmutz, M., Wu, Y., Hubbard, S.S., Cassiani, G., 2020. Time-lapse monitoring of root water uptake using electrical resistivity tomography and mise-à-la-masse: a vineyard infiltration experiment. *SOIL* 6, 95–114. <https://doi.org/10.5194/soil-6-95-2020>

McIvor, A.L., Spencer, T., Möller, I., Spalding, M., 2013. The response of mangrove soil surface elevation to sea level rise. *Nat. Coast. Prot. Ser. Rep. 3*. Cambridge Coastal Res. Unit Work. Pap. 42. ISSN 2050-7941.

McKee, K., Rogers, K., Saintilan, N., 2012. Response of salt marsh and mangrove wetlands to changes in atmospheric CO₂, climate, and sea level, in: *Global Change and the Function and Distribution of Wetlands*. https://doi.org/10.1007/978-94-007-4494-3_2

McKee, K.L., Cahoon, D.R., Feller, I.C., 2007. Caribbean mangroves adjust to rising sea level through biotic controls on change in soil elevation. *Glob. Ecol. Biogeogr.* 16. <https://doi.org/10.1111/j.1466-8238.2007.00317.x>

Meinzer, F.C., Brooks, J.R., Bucci, S., Goldstein, G., Scholz, F.G., Warren, J.M., 2004. Converging patterns of uptake and hydraulic redistribution of soil water in contrasting woody vegetation types. *Tree Physiol.* 24, 919–928.

Middleton, B., Devlin, D., Proffitt, E., McKee, K., Cretini, E.F., 2008. Characteristics of mangrove swamps managed for mosquito control in eastern Florida, USA. *Mar. Ecol. Prog. Ser.* 371, 117–129.

Musgrave, H., Binley, A., 2011. Revealing the temporal dynamics of subsurface temperature in a wetland using time-lapse geophysics. *J. Hydrol.* 396.

590 <https://doi.org/10.1016/j.jhydrol.2010.11.008>

591 Oldenburg, D.W., Li, Y., 1999. Estimating depth of investigation in DC resistivity and IP
592 surveys. *Geophysics* 64, 403–416. <https://doi.org/10.1190/1.1444545>

593 Parida, A.K., Jha, B., 2010. Salt tolerance mechanisms in mangroves: A review. *Trees* 24,
594 199–217.

595 Passioura, J. B., M. C. Ball, and J. H. Knight. 1992. Mangroves may salinize the soil and in
596 so doing limit their transpiration rate. *Functional Ecology*. 6, 4, 476-481.
597 <https://doi.org/10.2307/2389286>

598 Rada, F., Goldstein, G., Orozco, A., Montilla, M., Zabala, O., Azocar, A., 1989. Osmotic
599 and turgor relations of three mangrove ecosystem species. *Funct. Plant Biol.* 16, 477–
600 486.

601 Rey, J.R., O’Connell, S.M., Carlson, D.B., Brockmeyer Jr, R.E., 2009. Characteristics of
602 mangrove swamps managed for mosquito control in eastern Florida, USA: a re-
603 examination. *Mar. Ecol. Prog. Ser.* 389, 295–300.

604 Rey, J.R., Rutledge, C.R., 2009. Mosquito Control Impoundments. *Entomol. Nematol.*

605 Rey, J.R., Shaffer, J., Crossman, R., Tremain, D., 1990. Above-ground primary production
606 in impounded, ditched, and natural Batis-salicornia marshes along the Indian River
607 Lagoon, Florida, USA. *Wetlands* 10, 151–171.

608 Richards, J.H., Caldwell, M.M., 1987. Hydraulic lift: substantial nocturnal water transport
609 between soil layers by *Artemisia tridentata* roots. *Oecologia* 73, 486–489.

610 Robinson, J., Buda, A., Collick, A., Shober, A., Ntarlagiannis, D., Bryant, R., Folmar, G.,
611 Andres, S., Slater, L., 2020. Electrical monitoring of saline tracers to reveal subsurface
612 flow pathways in a flat ditch-drained field. *J. Hydrol.*
613 <https://doi.org/10.1016/j.jhydrol.2020.124862>

614 Sam, R., Ridd, P., 1998. Spatial variations of groundwater salinity in a mangrove-salt flat
615 system, Cocoa Creek, Australia. *Mangroves Salt Marshes* 2, 121–132.

616 Scholander, P.F., Hammel, H.T., Hemmingsen, E., Garey, W., 1962. Salt balance in
617 mangroves. *Plant Physiol.* 37, 722.

618 Scholz, F.G., Bucci, S.J., Guillermo, G., and Meinzer, F.C., Franco, A.C., 2002. Hydraulic
619 redistribution of soil water by neotropical savanna trees. *Tree Physiol.* 22, 603–612.

620 Singha, K., Gorelick, S.M., 2005. Saline tracer visualized with three-dimensional electrical
621 resistivity tomography: Field-scale spatial moment analysis. *Water Resour. Res.*
622 <https://doi.org/10.1029/2004WR003460>

623 Slater, L., Binley, A.M., Daily, W., Johnson, R., 2000. Cross-hole electrical imaging of a
624 controlled saline tracer injection. *J. Appl. Geophys.* [https://doi.org/10.1016/S0926-](https://doi.org/10.1016/S0926-9851(00)00002-1)
625 [9851\(00\)00002-1](https://doi.org/10.1016/S0926-9851(00)00002-1)

626 Slater, L., Zaidman, M.D., Binley, A.M., West, L.J., 1997. Electrical Imaging of Saline
627 Tracer Migration for the Investigation of Unsaturated Zone Transport Mechanisms.
628 *Hydrol. Earth Syst. Sci.* <https://doi.org/10.5194/hess-1-291-1997>

629 Slater, L.D., Sandberg, S.K., 2000. Resistivity and induced polarization monitoring of salt
630 transport under natural hydraulic gradients. *GEOPHYSICS.*
631 <https://doi.org/10.1190/1.1444735>

632 Smith III, T.J., Boto, K.G., Frusher, S.D. and Giddins, R.L., 1991. Keystone species and
633 mangrove forest dynamics: the influence of burrowing by crabs on soil nutrient status
634 and forest productivity. *Estuarine, coastal and shelf science*, 33(5), pp.419-432.

635 Stringer, C.E., Rains, M.C., Kruse, S., Whigham, D., 2010. Controls on water levels and
636 salinity in a barrier island mangrove, Indian River Lagoon, Florida. *Wetlands* 30, 725–
637 734.

638 Sumner, D.M., Belaine, G., 2005. Evaporation, precipitation, and associated salinity
639 changes at a humid, subtropical estuary. *Estuaries* 28, 844–855.

640 Sutter, E., Ingham, M., 2016. Seasonal saline intrusion monitoring of a shallow coastal
641 aquifer using time-lapse DC resistivity traversing. *Near Surf. Geophys.* 14, 1–15.
642 <https://doi.org/10.3997/1873-0604.2016039>

643 Twilley, R.R., Chen, R., 1998. A water budget and hydrology model of a basin mangrove
 644 forest in Rookery Bay, Florida. *Mar. Freshw. Res.* 49, 309–323.
 645 Urish, D.W., Frohlich, R.K., 1990. Surface electrical resistivity in coastal groundwater
 646 exploration. *Geoexploration* 26, 267–289.
 647 Vacher, H.L., Seale, L.D., Florea, L.J., Brinkmann, R., 2008. Using ALSM to map
 648 sinkholes in the urbanized covered karst of Pinellas County, Florida—2. Accuracy
 649 statistics. *Environ. Geol.* 54, 1007–1015.
 650 Wolanski, E., Mazda, Y., Ridd, P., 1993. Mangrove hydrodynamics. *Trop. mangrove*
 651 *Ecosyst.* 43–62.
 652
 653

Time Step	Start	End	Duration	Quadripoles		
1	<i>12:18:39</i>	<i>13:05:49</i>	<i>0:47:10</i>	<i>1219</i>	day 1	rising tide
2	13:46:05	14:32:37	0:46:32	1146		
3	18:45:29	19:31:38	0:46:09	1049		falling tide
4	19:32:57	20:19:34	0:46:37	1047		
5	20:29:51	21:16:41	0:46:50	1048		
6	21:20:37	22:08:00	0:47:23	1048		
7	0:01:16	0:47:28	0:46:12	1048	night	rising tide
8	3:09:18	3:57:04	0:47:46	1049		
9	4:40:01	5:26:26	0:46:25	1048		falling tide
10	6:38:22	7:26:26	0:48:04	1049		
11	7:44:00	8:30:43	0:46:43	1045	day 2	
12	8:34:44	9:22:03	0:47:19	1049		
13	10:45:12	11:34:33	0:49:21	1045		

*Table 1 Data acquisition schedule. Only time steps that shown significant change (**bold**) from the initial time step (*italics*) are presented in this paper.*

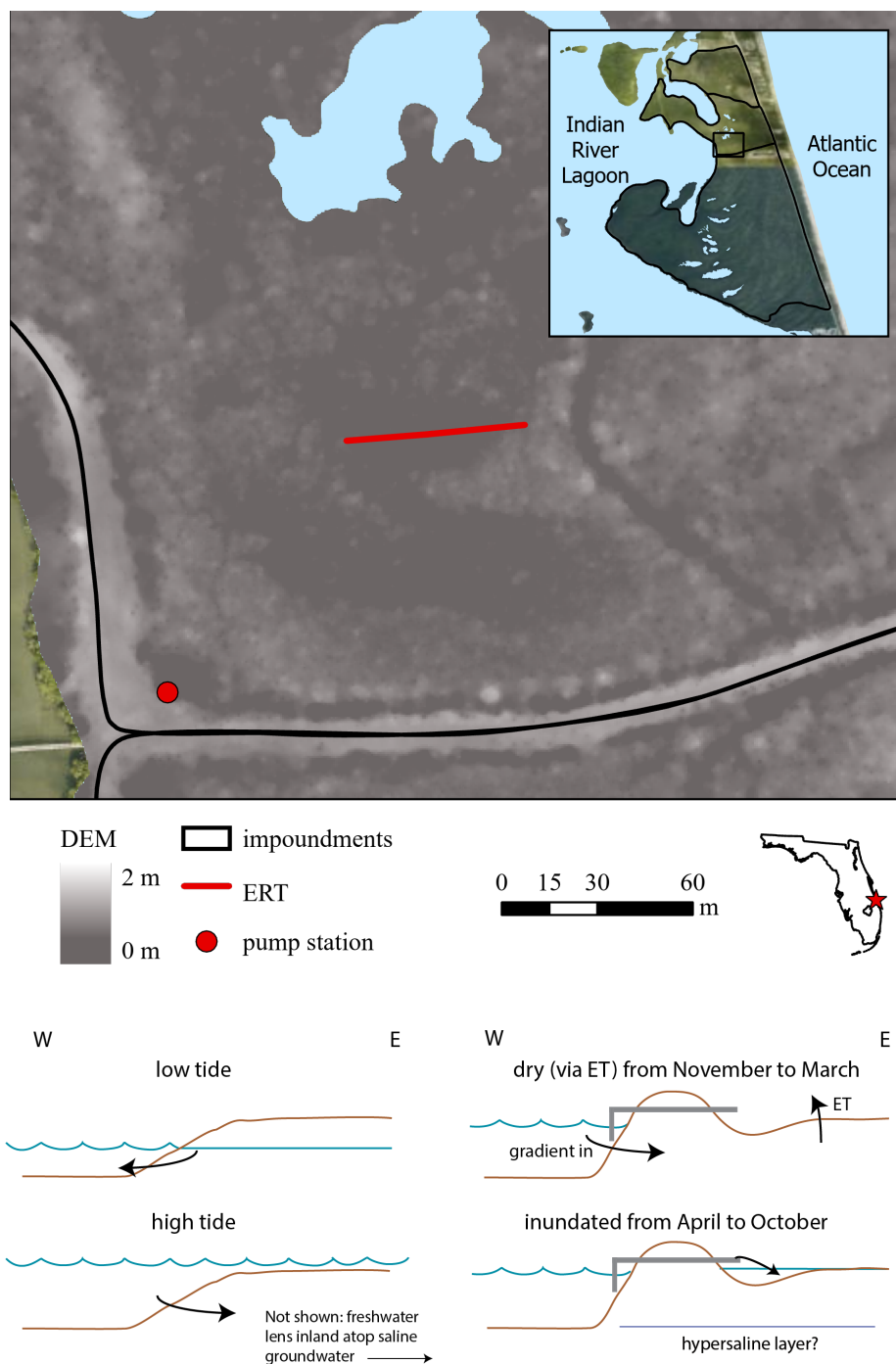


Figure 1 Top: Digital elevation map of Imp-24: a mosquito-control impoundment on the west side on North Hutchinson Island, Florida, USA. Bottom: Cross-sectional schematic of free flowing system verses an impounded system at the study site including the current inundation schedule. The impoundment is an earthen dike that prevents surface water exchange between impoundments to the north and south and the brackish, tidal lagoon to the west. Impoundment water levels are measured at the pump station (not shown), which is in a trench between the dike and mangrove forest.

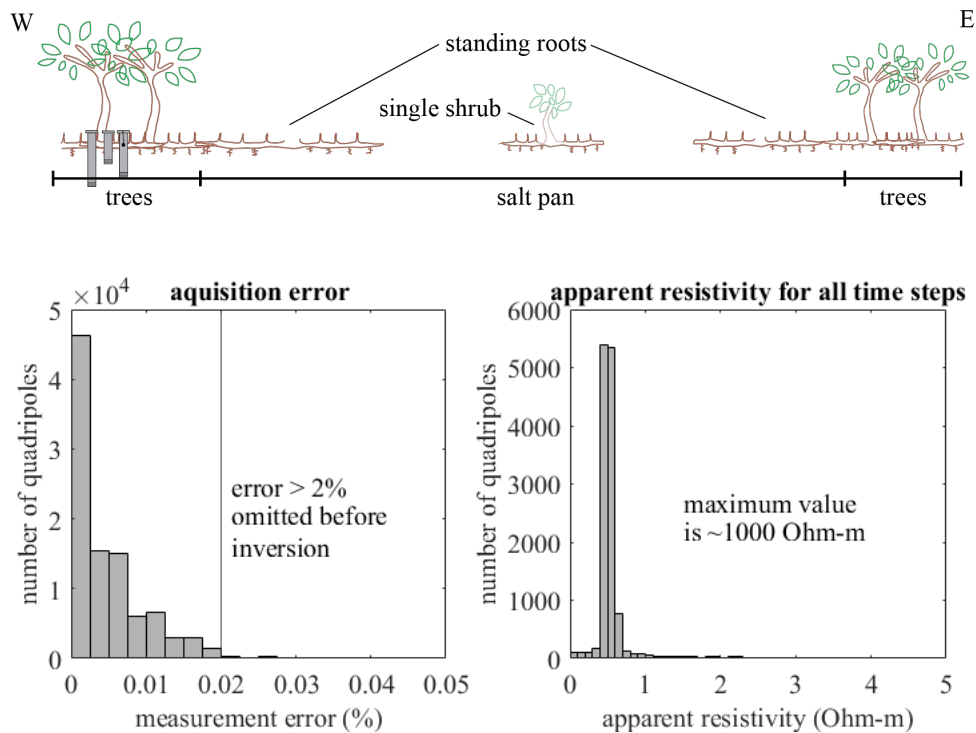


Figure 2 Top: ERI transect crosses through small-stature mangrove trees and a salt flat with a single mangrove shrub. Bottom: Histograms of ER instrument acquisition error and apparent resistivity from all timesteps.

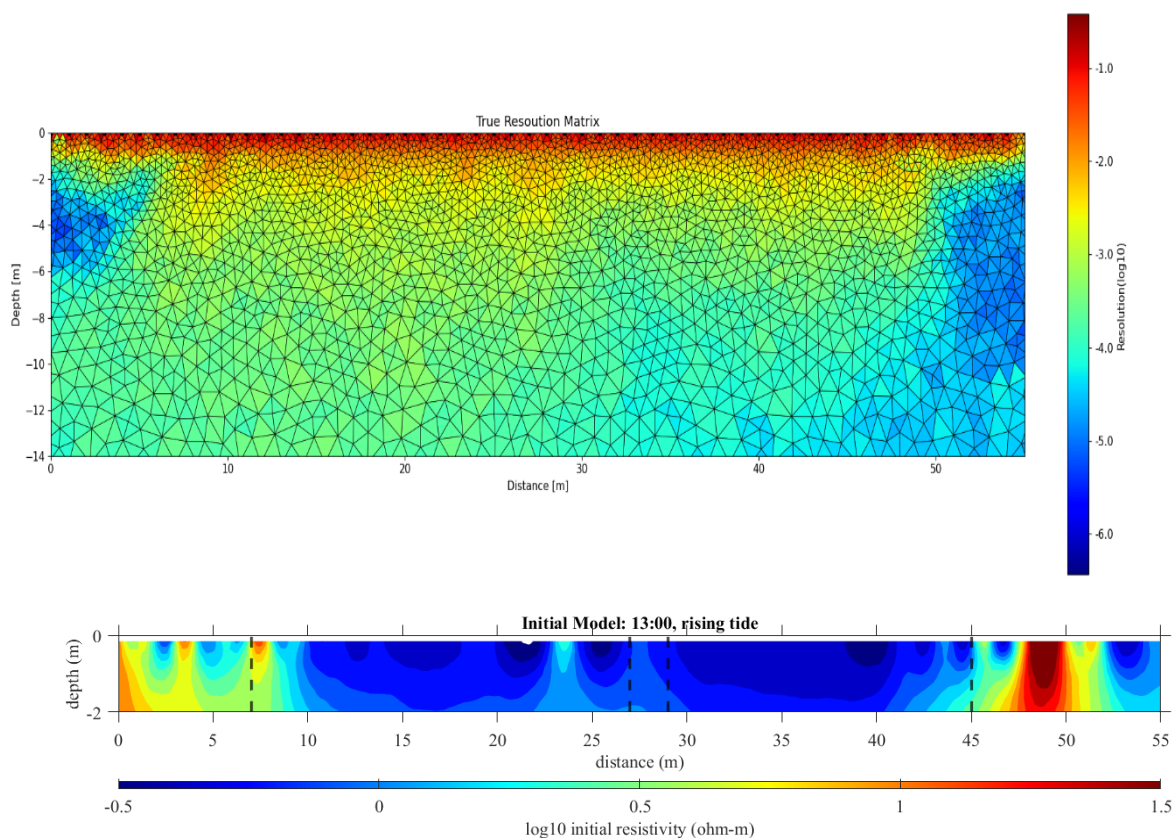


Figure 3 Top: True resolution matrix calculated for the first time step. The best resolution is in the first two meters of the subsurface. The very low resolution at the edges (blue) are areas without data coverage. Bottom: 22°C equivalent resistivity of the first two meters from the first time step (day 1, 13:00.) Black dashed lines delineate the boundary between tree groupings and the salt flat with scattered standing roots. The salt flat is an order of magnitude less resistive than the vegetated zones on either side. The whole profile exhibits very low resistivity values indicative of the hypersaline and wet environment.

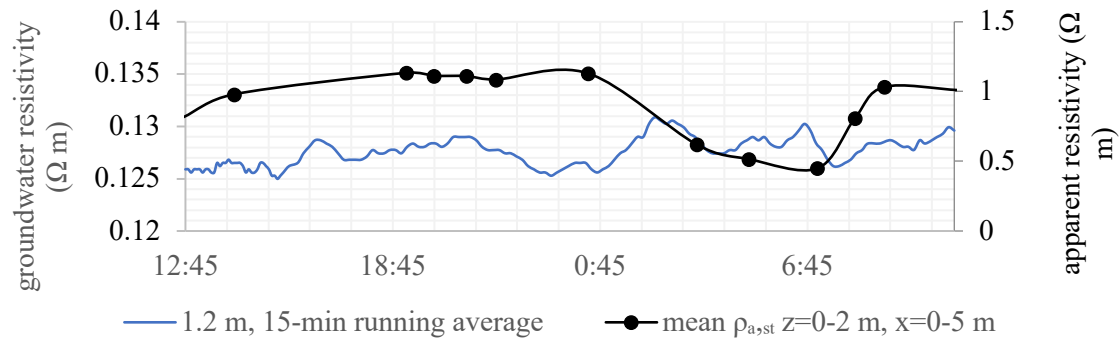
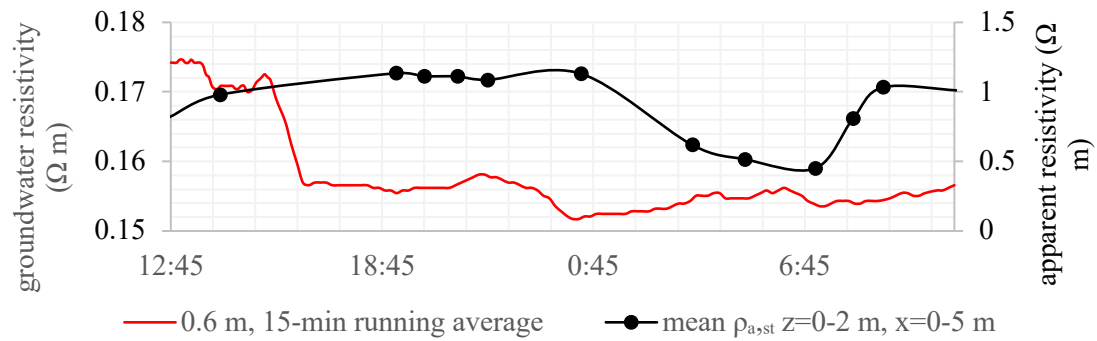
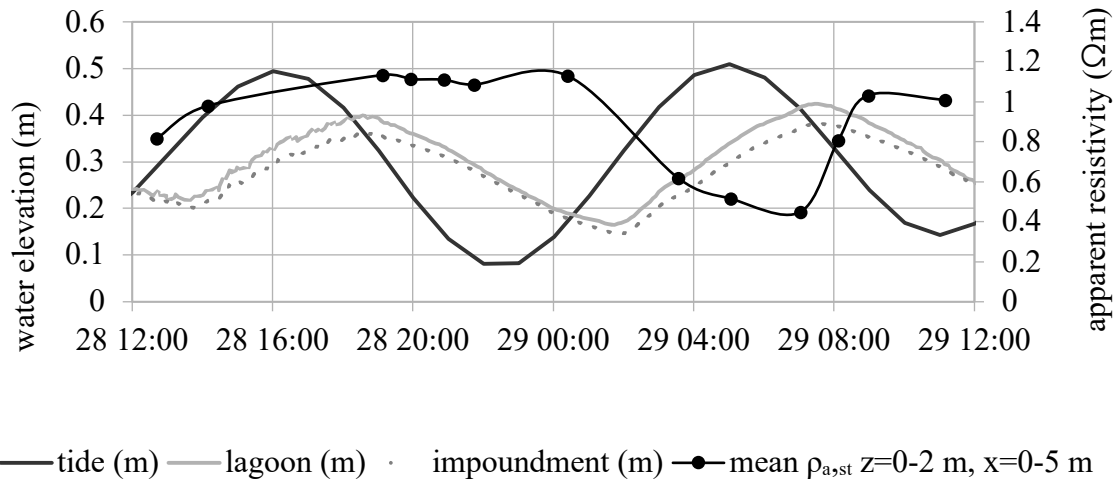


Figure 4 Water measurements during the resistivity survey and raw ERI measurements. The 22°C equivalent mean apparent resistivity ($\rho_{a,st}$) from the top 2 meters for each time step plotted with tidal cycle (top) recorded in the lagoon, the trench between the earthen dike and mangrove forest, and an inlet to the south. The 22°C equivalent mean apparent resistivity ($\rho_{a,st}$) for each time step (from the top 2 meters and first 5 meter along the transect) plotted with a 15-min running average of groundwater resistivity at 0.6 m depth (middle) and 1.2 m depth (bottom).

661

662

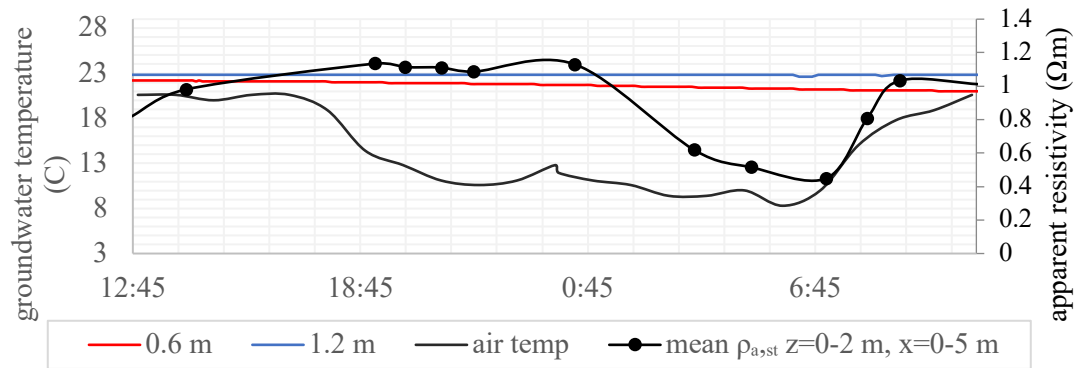


Figure 5 Air temperature plotted with groundwater temperature at 0.6 and 1.2 meters depth and the 22°C equivalent mean apparent resistivity ($\rho_{a,st}$) from the top 2 meters of each time step.

663

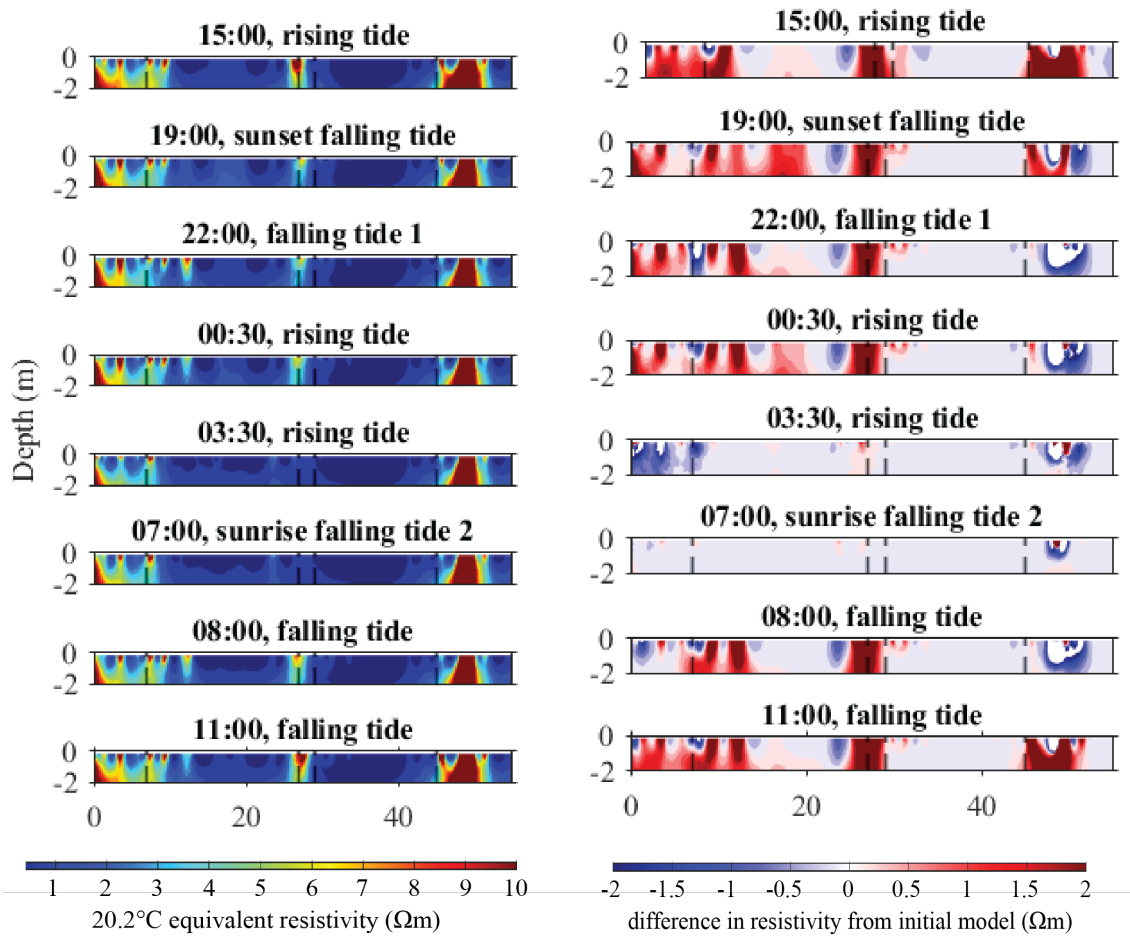


Figure 6 Selected profiles from the time lapse survey. Profiles on the left display 22°C equivalent resistivity (ρ_{st}) for a given time step. Profiles on the right display the resistivity difference from the initial model collected at approximately 13:00 on day 1 (rising tide). Black dashed line delineate vegetation zones: dense scrub mangrove trees cover the east and west end of the transect (0-7 m and 45-55 m, respectively); a salt flat with some standing roots define much of the center of the profile. A single scrub tree is in the middle of the salt flat at approximately 29 m.

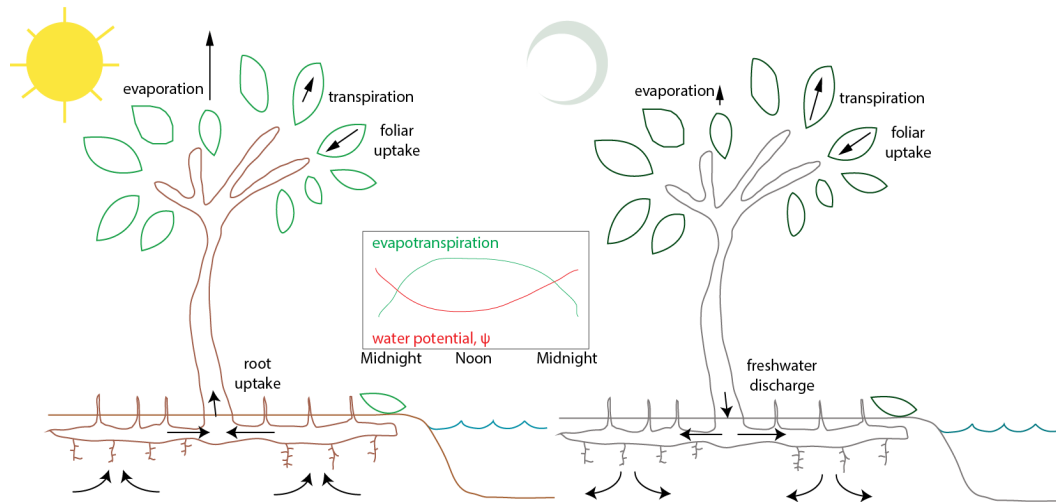


Figure 7 Suggested diel salt cycle for a black mangrove as suggested by time-lapse ERI results. The cycle contains a period of water uptake that slows down at sunset. Water pressure potential in the roots increases enough for water and salts to flow back into the soil (hydraulic redistribution.) Hydraulic redistribution starts before midnight and continues until sunrise. Transpiration and foliar uptake rates will depend on Original image from Alongi and Brinkman (2011).